Int. J. Multiphase Flow Vol. 15, No. 6, pp. 925–935, 1989
Printed in Great Britain.

0301-9322/89 $3.00 + 0.00

ENTRAINMENT AND CONDENSATION EFFECTS IN THE UPWARD ACCELERATION OF A LIQUID COLUMN

J. S. SEO[1]† and S. G. BANKOFF[2]

Departments of [1]Mechanical and [2]Chemical Engineering, Northwestern University, Evanston, IL 60208-3120, U.S.A.

(*Received* 28 *October* 1987; *in revised form* 20 *March* 1989)

Abstract—The instability-governed entrainment rate of the lower surface of a subcooled water column accelerated upwards by an expanding steam mass is measured. It is found that the entrainment rate is approximately proportional to the fourth root of the acceleration. This would be the case if the characteristic length scale in the late stages of Taylor instability were governed by linear instability theory. In addition to the linear displacement measurements, the steam pressure in the lower driver section was monitored as a function of time. Estimates of the concentration, radius and age distribution of the entrained droplet population were made by modeling the bubble-and-spike breakup into discrete droplets. This allows the steam condensation rate, and hence the steam pressure, at each instant of time to be computed. This is compared with the observed steam pressure history. Reasonable agreement is found. One can thus estimate the reduction in work potential in the case of a steam explosion in the lower plenum of a pressurized-water nuclear reactor.

Key Words: Taylor instability effects

INTRODUCTION

The interesting effects of Rayleigh–Taylor instability of a liquid–gas interface lie in the nonlinear domain, where the well-known bubble-and-spike wave shape initially appears. Indeed, most important effects occur after this stage, when the spikes begin to break up into droplets and enter the lighter phase. It is at this point that rapid interfacial mass and heat transfer can occur. One practical example is the possibility of a vapor explosion in the lower plenum of a pressurized-water reactor in the course of a severe accident. The exploding mixture pushes upward on a liquid column, which may be primarily water or fuel, depending upon the location of the exploding mixture. This liquid column would impact on the upper head of the vessel, possibly with head failure. The work potential, however, may be greatly modified by the entrainment of liquid droplets from the upward-moving column into the expanding gaseous mixture. If the droplets are water, condensation will result, with a consequent reduction in work potential. If the droplets are molten fuel/steel, further vaporization and an increase in work potential may result. Similar considerations apply to the liquid-metal fast breeder reactor. Rapid mixing owing to Taylor instability can also occur in other technical phenomena, such as inertially-confined fusion. There is, thus, a real incentive to study the details of these interactions, both experimentally and analytically.

Linear theories of Rayleigh–Taylor instability (Rayleigh 1900; Taylor 1950; Bellman & Pennington 1954; Bankoff 1959; Hsieh 1979; Taghavi-Tafreshi & Dhir 1980) are applicable for short times only. Nonlinear Taylor instability has therefore been the subject of a number of investigations (Lewis 1950; Birkhoff 1954; Emmons *et al.* 1960; Ratafia 1973; Christopher 1977; Corradini 1978; Tobin & Cagliostro 1978; Read & Young 1983). Of particular interest relative to reactor safety was the work of Christopher (1977), who investigated the transient development of air discharges, liquid–vapor discharges and combined discharges into a liquid pool. Taylor instability was seen in the upper pool interface of all the runs as the pool decelerated. Large entrainment rates were calculated to occur during the two-phase discharge. A rough convective heat transfer coefficient was calculated, in view of the uncertainty in the initial quality and unresolved input parameters. For saturated liquid–vapor discharge, $h = 1.1 \times 10^6$ W/m^2 K; and for saturated liquid discharge,

†Present address: Korea Military Academy, Seoul 139-799, Korea.

$h = 1.1 \times 10^7\ \mathrm{W/m^2\,K}$. These extremely high heat transfer coefficients are in the same range as measurements by Bankoff & Mason (1962) of condensation heat transfer coefficients on growing and collapsing bubbles in subcooled boiling.

An extension of the Dienes (1978) energy method to two incompressible fluids with interfacial mass transfer was made by Chang & Bankoff (1983, 1984). They showed that the vapor phase, with or without surface condensation, does not affect the character of the nonlinear Taylor instabilities in any important way. Their formulation predicts infinite spike velocities in very small times (10^{-3}–10^{-4} s for 100 G). Annular Taylor waves in a circular pipe were also considered. The existence of these waves was confirmed by top-view photographs taken by Jacobs *et al.* (1985), who performed air–water downwards-acceleration experiments in a vertical circular tube. The disturbances observed were axisymmetric, with wavelengths corresponding closely to the linear fastest-growing values.

The closest previous work to the present study was that of Chang-Mateu (1985), who performed nitrogen–water upward-acceleration experiments in a 0.1 m dia tube at 30–200 g. A single scored diaphragm burst open in flower-petal fashion to initiate the motion, giving rise to a Taylor bubble at the lower liquid interface. The erosion of the lower interface of the water column was determined by high-speed photography through measurement of the relative velocity, V_r, of the upper and lower interfaces. The data were better fitted by a square-root dependency of V_r on the acceleration than a fourth-root dependency. However, it seems possible that the early appearance of the Taylor bubble was due to the central gas jet produced by the flower-petal opening of the diaphragm. Consequently, one objective of the present work is to extend the Chang-Mateu work to the steam–water system under conditions where the initial lower column interface is nearly flat, and thereby to determine the dependency of the liquid entrainment rate on the mean acceleration. Estimates are made of the steam condensation rates, and hence the reduction in mechanical work performed by the expanding steam.

EXPERIMENT

A vertical low-pressure shock tube assembly, shown in figure 1, is used to investigate the entrainment and condensation effects due to Taylor instability.

As shown in figure 2, the shock tube consists of three parts, a lower driver section, an intermediate vacuum chamber and an upper driven section. The lower section, made of stainless steel pipe, 0.1 m i.d. and 0.94 m long, is separated from the vacuum chamber above by a relatively strong diaphragm (double or triple layers of 0.125 mm thick aluminum foil). In order to generate steam, four mica-insulated band heaters (650 W each) are wrapped around the pipe outer wall. A pneumatic piston-type plunger, with a cutter for rupturing the strong diaphragm, is housed at the bottom of the section. The 0.1 m long vacuum chamber, which is separated by a weak diaphragm (0.025 mm thick aluminum foil) from the upper section, prevents condensation on the underside of the weak diaphragm prior to rupture.

High-speed motion pictures of both the upper and lower interfaces of the water column are taken in the upper section, which consists of a 95 mm i.d. and 0.91 m long transparent polycarbonate tube. Two perforated plates are placed between the upper section and the vacuum chamber, with the weak diaphragm between them, in order to get a flat initial lower interface.

An instrumentation and data acquisition diagram is shown in figure 3. Two pressure histories, one of steam pressure in the driver section and the other just above the weak diaphragm, are obtained from the pressure transducers and stored in a micro-computer. These are charge-output pressure transducers with a resonance frequency of 250 kHz and rise time of 2 μs. A water-cooled adapter is used for the steam-side pressure transducer in order to insulate it from the wall temperature. The outputs from the pressure transducers are fed into the charge amplifiers. A data sampling program is utilized to store the pressure data on a floppy disk. The sampling time interval is 24.5 μs.

A 16 mm Photec IV-A high-speed movie camera, with a Mamiya 100 mm f/2.7 lens, is used at 2000 or 4000 frames/s. Four 150 W spot lamps are placed behind the test section to illuminate the rising water column.

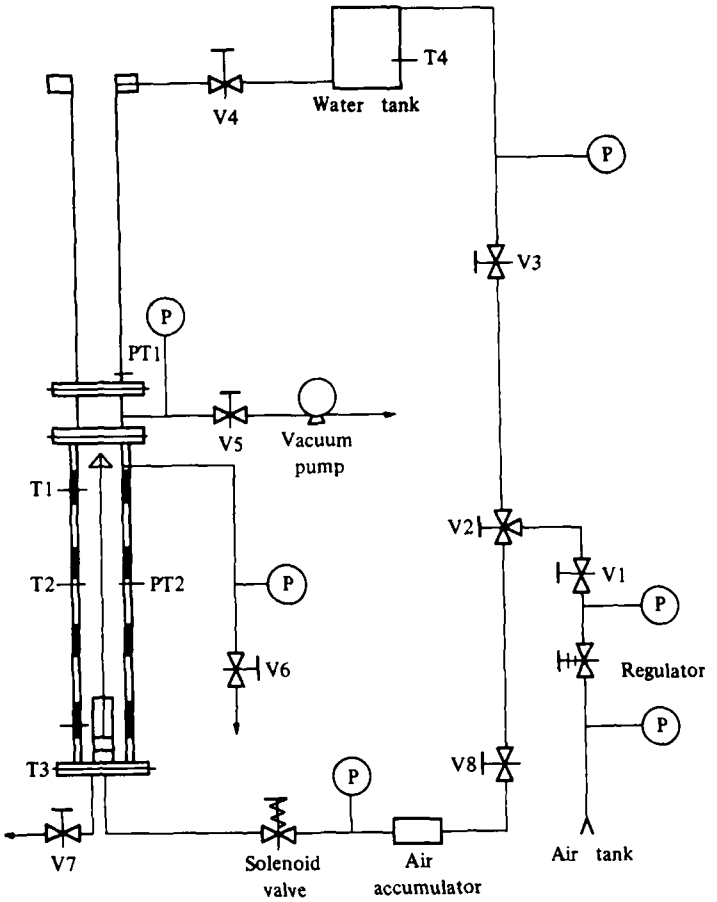

Figure 1. Schematic diagram of the shock tube assembly.

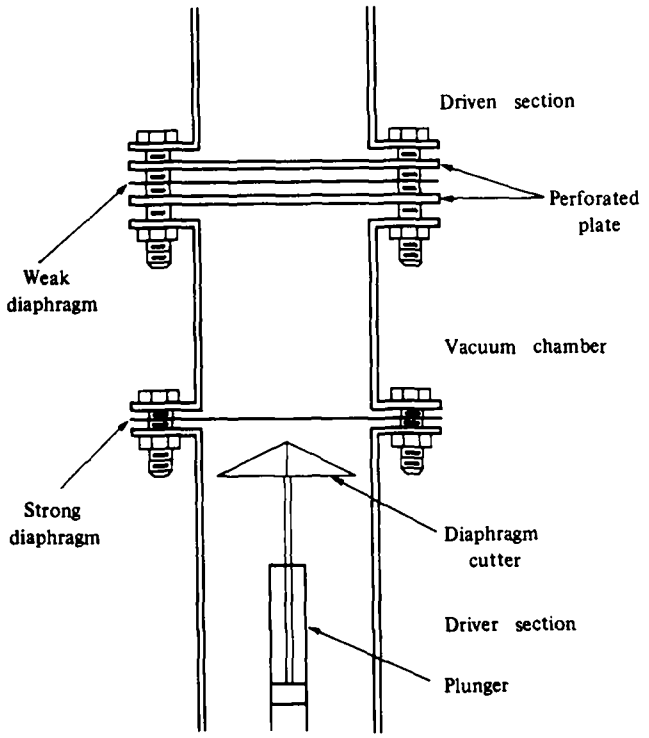

Figure 2. Details of the placement of the two diaphragms.

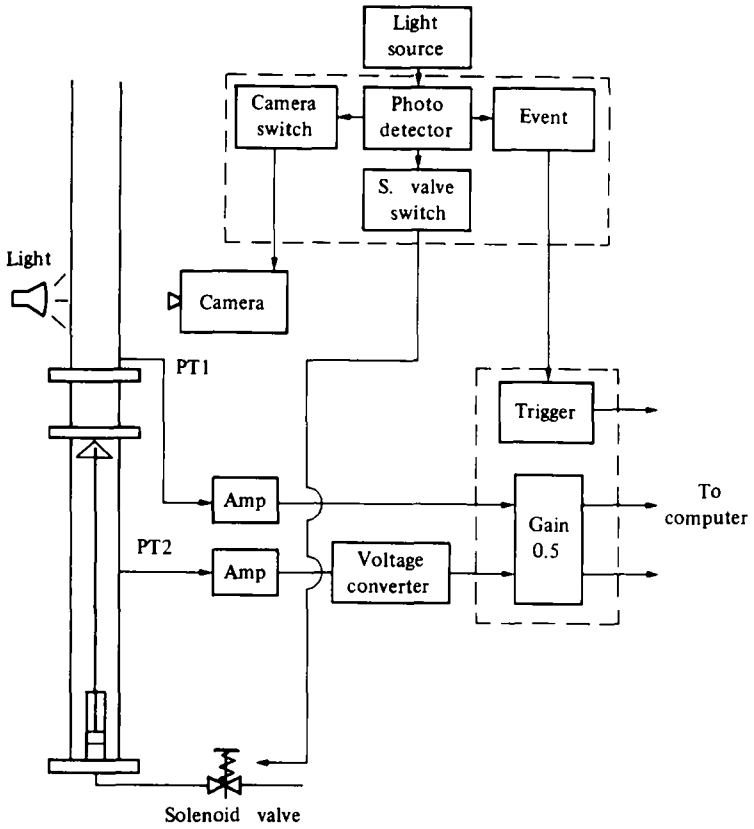

Figure 3. Data acquisition diagram.

The experiment is started by pouring 2 l. of water into the lower section. The equipment is then assembled, and the vacuum chamber is evacuated to 0.033 MPa. The lower section is then heated by the band heaters. To eliminate air in the lower section, steam is vented three or four times when the steam pressure is at about 0.17 MPa. When the predetermined steam pressure is reached, the desired amount of water is placed above the weak diaphragm, and excess water in the lower section is drained out. The light beam source in the trigger box is then cut off, which activates the solenoid valve and high-speed camera, and triggers the sampling circuit simultaneously. The water column is accelerated upwards, following rupture of the diaphragms upon opening the solenoid valve. During this time photographs are taken and pressure data are collected.

From the high-speed motion pictures, the heights of the upper and lower interfaces, and hence the water column height, are measured as functions of time (figure 4). It was found that the upper interface of the water column is flat through the period of interest, except for the final stage. All lower interfaces that were not flat depended upon the rupture shape of the weak diaphragm. Hence, only photographs that showed a flat lower interface were chosen.

ENTRAINMENT VELOCITIES

The velocity of the lower interface relative to the upper interface is called the entrainment velocity. The data for the elevation of the upper interface and height of the water column were fitted by polynomials in time. The coefficients of the third order for the upper interface, and of the second order for the column height, were small enough to be neglected. Thus, constant accelerations and entrainment velocities were obtained. Typical experimental data and polynomial fits of the upper level and column height are shown in figure 5. Complete data are given in Seo (1987).

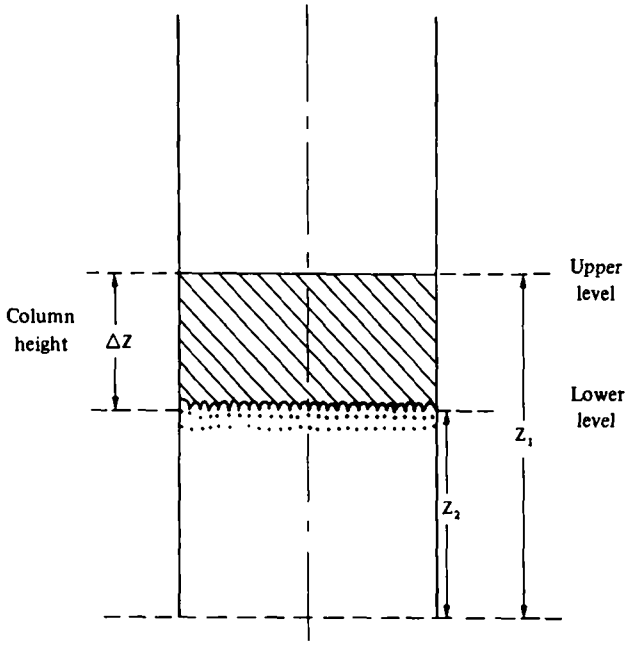

Figure 4. Definition of water level measurement.

The experimental conditions and results are listed in table 1. The acceleration varies from 25.8 to 346 g. The entrainment velocity data can be expressed as a two-parameter least-squares fit passing through the origin by

$$V_r = 1.22\, a^{(0.232 \pm 0.100)}. \quad [1]$$

It is thus seen that the best exponent is close to 0.25, which corresponds to a characteristic length being given by the fastest-growing wavelength, rather than the tube diameter. The square-root dependency has, on dimensional grounds, the tube diameter as the characteristic length. On the other hand, the fourth-root dependency corresponds, from linear stability arguments, to a characteristic length scale which is proportional to the fastest-growing wavelength.

This result confirms those of several previous studies. Air–water experiments performed by Lewis (1950), in a rectangular geometry (6.35 × 12.7 mm), over a range of downwards accelerations from 3.0 to 140 g, resulted in the following correlation:

$$V_r = C_1\sqrt{a\lambda_0}, \quad [2]$$

where λ_0 is the observed wavelength. Emmons *et al.* (1960) obtained a similar result in a rectangular test section (127 × 25.4 mm), with air–methanol, except for the coefficient C_1. Corradini (1978),

Table 1. Summary of experimental results

Expt No.	Driver pressure (MPa)	Initial liquid height, Z_1(mm)	Dimensionless acceleration (a/g)	Relative velocity, V_r(m/s)	Liquid temp., T_L(°C)
702	0.377	65	75.4	4.06	20
707	0.377	65	188	6.31	100
709	0.466	60	135	5.03	24
712	0.481	80	123	4.59	29
714	0.515	100	138	6.54	27
721	0.377	60	346	7.12	100
726	0.377	70	65.5	5.03	27
727	0.515	60	153	6.06	26
728	0.446	60	234	7.63	100
729	0.377	100	112	6.22	100
730	0.515	60	332	6.85	100
732	0.343	80	52.6	4.71	100
733	0.412	70	25.8	4.28	24
734	0.412	70	138	6.07	100

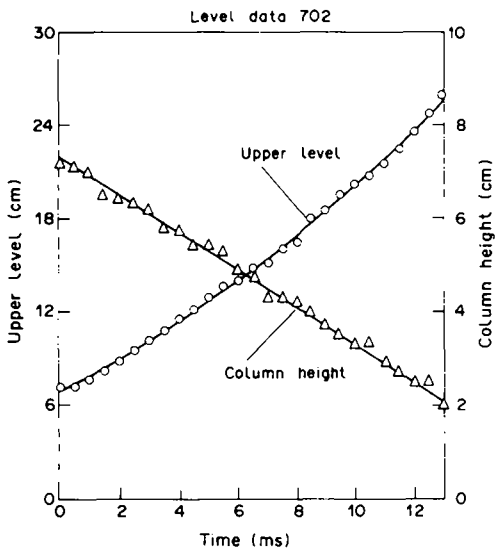

Figure 5. Height of upper water surface and water column height for run 702.

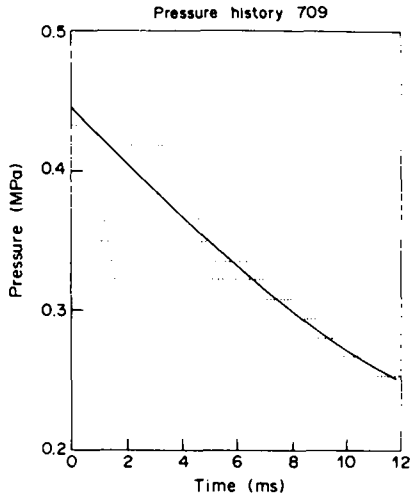

Figure 6. A typical pressure history.

whose experiment was performed with air–water in a flat-plate geometry (127 × 19 mm), found his best-fit two-parameter correlation to be

$$V_r = 0.54\, a^{(0.332 \pm 0.27)}, \quad [3]$$

but this may be related to the large aspect ratio of his test section.

Chang-Mateu (1985), using a 0.1 m i.d. tube with nitrogen–water, found that the best correlation, such that $V_r = 0$ when $a = 0$, was

$$V_r = 0.0186\, a^{0.57 \pm 0.11}. \quad [4]$$

However, these experiments differed from the present experiments in that the liquid column initially rested directly on the strong diaphragm. The unfolding of the diaphragm upon rupture into flower-petal form resulted in a central gas jet for small times, which caused the lower liquid interface to resemble a Taylor bubble. In the present series the central jet was avoided by placing a perforated plate below and above the weak diaphragm. This resulted in a nearly flat lower liquid interface in nearly all cases for the first three tube diameters of upwards travel. Since the acceleration is nearly constant, one would expect the Taylor bubble to be the stable, long-term shape in the absence of entrainment. This suggests that entrainment of droplets into the vapor space may stabilize an initially-flat interface contained in a round tube, or at least slow down the transition to the Taylor buble form. A longer tube length would be required to examine this hypothesis. As noted above, the Taylor bubble form corresponds to a square-root dependency of the relative gas–liquid mean velocity on the acceleration, while the flat interface gives a fourth-root dependency, if the characteristic length scale is the fastest-growing wavelength of linear theory. Hence, present results suggest that the linear theory has a strong relationship to the wavelength of the late stages of repetitive nonlinear spike growth and tip breakup.

CONDENSATION RATE MODEL

When the subcooled water droplets, formed by breakup of the Taylor spikes, are entrained into the expanding steam, transient heat transfer occurs. This heat transfer is analyzed under the following assumptions:

(1) The water droplets are spherical and their diameter is constant, since the acceleration is nearly constant.
(2) The thermophysical properties of the water droplets are constant.
(3) The steam remains saturated during the expansion.
(4) Convection and radiation of heat are neglected.

(5) Mechanical and viscous dissipation terms in the energy conservation equation are negligible compared to thermal energy transport.
(6) The critical Weber number, We_{cr}, for droplet breakup is given by

$$We_{cr} = \frac{\rho_G v_{rel}^2 D_d}{\sigma} = 7 - 20, \qquad [5]$$

where v_{rel} is the relative velocity between the droplet and steam and σ is the surface tension. Taking the droplet diameter to be half of the fastest-growing wavelength, all We in these experiments, based on the initial relative velocity, are about 2. Hence, the droplets do not break up.

The local heat transfer rate from the steam to the water droplets is

$$\dot{q}_d(t) = h_{ov}(t) n(t) \pi D_d^2 (T_{sat}(t) - T_L), \qquad [6]$$

where $h_{ov}(t)$ is the overall heat transfer coefficient to the droplets, $T_{sat}(t)$ is the saturation steam temperature at the measured pressure, $p(t)$, T_L is the droplet temperature, D_d is the droplet diameter and $n(t)$ is the number of entrained droplets.

From a consideration of the relative magnitudes of the gas-side and liquid-side thermal resistances, it is readily found that the liquid-side resistance dominates. The liquid surface temperature varies with time, and can be fitted by a second-order polynomial in time. Assuming that convective effects within the droplet can be neglected, the problem reduces to a spherically-symmetric heat conduction problem:

$$\frac{\partial T}{\partial t} = \alpha \nabla^2 T, \qquad 0 \leqslant r < r_d, \qquad [7]$$

where α is the liquid thermal diffusivity and r_d is the droplet radius. The initial condition is

$$T = T_L \qquad \text{at } 0 \leqslant r \leqslant r_d, t = 0, \qquad [8]$$

and the boundary conditions are

$$T = T_L \qquad \text{at } r = 0 \qquad [9]$$

$$T = T_{sat}(t) \qquad \text{at } r = r_d. \qquad [10]$$

Assuming that

$$T_s(t) - T_L = C_0 + C_1 t + C_2 t^2, \qquad [11]$$

the temperature gradient at the droplet surface, $r = r_d$, is found to be

$$\left.\frac{\partial T}{\partial r}\right|_{r=a} = \frac{2C_0}{a} \sum_{n=1}^{\infty} \exp\left(-\frac{\alpha n^2 \pi^2 t}{a^2}\right) + \frac{C_1 a}{3\alpha} - \frac{2C_1 a}{\alpha \pi^2} \sum_{n=1}^{\infty} \frac{1}{n^2} \exp\left(-\frac{\alpha n^2 \pi^2 t}{a^2}\right)$$
$$+ \frac{2C_2 a t}{3\alpha} - \frac{4C_2 a^3}{\alpha^2 \pi^4} \sum_{n=1}^{\infty} \frac{1}{n^4} + \frac{4C_2 a^3}{\alpha^2 \pi^4} \sum_{n=1}^{\infty} \frac{1}{n^4} \exp\left(-\frac{\alpha n^2 \pi^2 t}{a^2}\right). \qquad [12]$$

Since there is an age distribution of droplets at any time t, an average temperature gradient at $r = a$ is calculated for all droplets:

$$\left.\overline{\frac{\partial T}{\partial r}}\right|_{r=a} = \frac{1}{t} \int_0^t \left.\frac{\partial T(t-\tau, r)}{\partial r}\right|_{r=a} d\tau$$
$$= \frac{2C_0 a}{\alpha \pi^2 t} \sum_{n=1}^{\infty} \frac{1}{n^2} \left[1 - \exp\left(-\frac{\alpha n^2 \pi^2 t}{a^2}\right)\right] + \frac{C_1 a}{3\alpha}$$
$$- \frac{2C_1 a^3}{\alpha^2 \pi^4 t} \sum_{n=1}^{\infty} \frac{1}{n^4} \left[1 - \exp\left(-\frac{\alpha n^2 \pi^2 t}{a^2}\right)\right] + \frac{C_2 a t}{3\alpha}$$
$$- \frac{4C_2 a^3}{\alpha^2 \pi^4} \sum_{n=1}^{\infty} \frac{1}{n^4} + \frac{4C_2 a^5}{\alpha^3 \pi^6 t} \sum_{n=1}^{\infty} \frac{1}{n^6} \left[1 - \exp\left(\frac{\alpha n^2 \pi^2 t}{a^2}\right)\right], \qquad [13]$$

where τ is the birth time of the droplets. The average droplet heat transfer coefficient is then

$$h_{d,av}(t) = k \left.\frac{\overline{\partial T}}{\partial r}\right|_{r=a} \frac{1}{[T_{sat}(t) - T_L]}, \quad [14]$$

where k is the thermal conductivity. For comparison, average droplet heat transfer coefficients are also calculated, assuming that the droplet surface temperature remains constant at the initial saturation temperature.

EXPERIMENTAL HEAT TRANSFER COEFFICIENT

From the experimental steam pressure and level data, the experimental heat transfer coefficient can be determined as a function of time:

$$h_{exp}(t) = \frac{\dot{m}_G(t) i_{LG}(t)}{A_{tot}(t)[T_{sat}(t) - T_L]}, \quad [15]$$

where $\dot{m}_G(t)$ is the rate of steam mass condensation and $A_{tot}(t)$ is the total heat transfer area. The number of droplets $n(t)$, can be determined under the assumption that the volume of the liquid film adhering to the driven section wall is negligible:

$$n(t) = \frac{6A_p \int_0^t V_r \, dt}{\pi D_d^3}, \quad [16]$$

where A_p is the cross-sectional area of the tube.

The total heat transfer area for condensation is the sum of the total surface area of the spikes, A_s, the wetted area on the driven section wall, $A_w(t)$ and the total surface area of the droplets, $A_d(t)$. The early stage heat transfer is dominated by $A_s + A_w$, whereas A_d is dominant in the late stage. Assuming the mean spike shape to be a sine wave of amplitude λ_m, the total surface area of the spike can be expressed as

$$A_s = 4A_p. \quad [17]$$

The wetted area on the driven section wall is obtained from the measurement of the lower column interface height, $Z_2(t)$:

$$A_w(t) = \pi D_p Z_2(t). \quad [18]$$

The droplet area is simply

$$A_d(t) = n(t)\pi D_d^2. \quad [19]$$

The steam pressure data are affected by shock waves, expansion waves and reflected waves, due to double diaphragms, in the early stages (figure 6). Therefore, a data-smoothing program, using cubic splines, is employed. From the smoothed-pressure data, the saturated enthalpies, $i_L(t)$ and $i_G(t)$, and the density of steam, $\rho_G(t)$, are derived:

$$\rho_G(t) = 5.08\, p(t)^{0.936} \quad [20]$$

$$i_G(t) = 2.78 \times 10^6\, p(t)^{0.0168} \quad [21]$$

and

$$i_L(t) = 7.75 \times 10^5\, p(t)^{0.267}, \quad [22]$$

where $p(t)$ is in MPa. The saturation temperature $T_{sat}(t)$ is obtained by interpolation in a steam table. The mass of steam as a function of time is thus obtained and is fitted to a second-order polynomial in time. Upon differentiation, this yields $\dot{m}_G(t)$, which can be substituted into [15], along with [16]–[22], to obtain the experimental heat transfer coefficient, $h_{exp}(t)$.

Typical values of the experimental heat transfer coefficient and average-droplet heat transfer coefficients, based on variable surface temperature, [11]–[14], and constant surface temperature, are plotted in figures 7 and 8. Other results are given in Seo (1987). The experimental values vary from about 7 to 400 kW/m^2 K, while the values from the two models vary from about 15 to

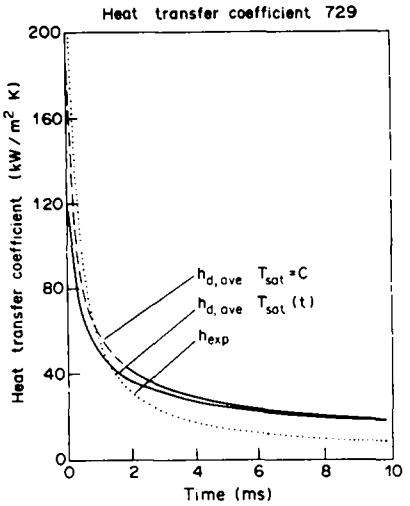

Figure 7. Heat transfer coefficients of run 729.

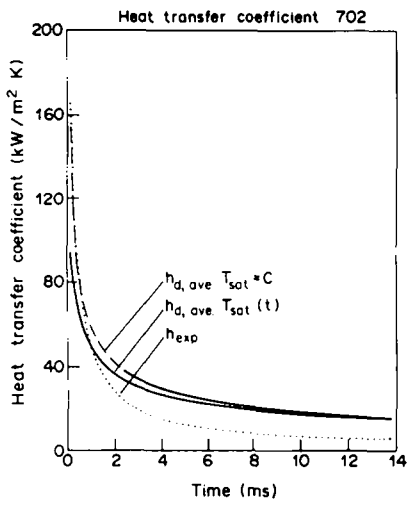

Figure 8. Heat transfer coefficients of run 702 (table 1).

250 kW/m² K. Despite the simplifying assumptions for both the model development and data analysis, it is seen that the experimental values and the two liquid-side heat transfer coefficients are in quite good agreement.

For short times, the experimental value is larger than both models, and in the late stage the experimental value is smaller than the modeled values. The disparity probably is principally due to the uncertainty of the estimation of spike length, breakup time and Sauter-mean droplet diameter. The differences between the experimental and modeled values in the late stage are about a factor of 2. This could originate from the estimate of the droplet diameter. The surface area of the droplets is 15–30 times larger than that of the spikes and the wetted wall in the late stage. If the droplet diameter estimate is optimized to give minimum least-square deviation of the variable surface-temperature heat transfer coefficient from the experimental heat transfer coefficient, the optimal-estimate diameter is $0.72\,\lambda_m$, where λ_m is the fastest-growing linear wavelength.

This seems high, because of the well-known bubble-and-spike shape of nonlinear Taylor instability, as well as the formation of satellite droplets. However, surface tension effects, as well as noncondensable gas effects on the condensation rate, which would be expected to be important in the later stages, may explain this late-time discrepancy. Initially, the air in the evacuated intermediate section contributes about 10^{-3} mol fraction to the condensing steam–air mixture. The early-time under-estimate probably derives from the smoothing of the pressure–time history. Initially, the pressure falls much more rapidly than the smoothed estimate, and hence the temperature driving force for condensation is greater than estimated. The ratio of the actual work, given by the area under the pressure–volume curve, to the ideal work of an adiabatic, reversible, constant-mass expansion is about 27% for an initial water temperature of 20°C, and about 38% for 100°C water. This compares with values of 24% with steam and room-temperature water found by Tobin & Cagliostro (1978) in a different geometry. With a noncondensable gas (nitrogen) Tobin & Cagliostro obtained a mechanical energy efficiency of 66%, while Chang-Mateu (1985) obtained an efficiency of nearly unity. There is thus substantial reduction in work potential, resulting from steam condensation.

DISCUSSION

This is a difficult experiment, since the actual spike shapes and droplet size distributions cannot be measured in this geometry. As noted above, we have modeled the droplet entrainment process by taking the droplet diameter to be constant, wherein reality there is undoubtedly a range of droplet sizes. The droplet diameter is assumed to be closely related to the fastest-growing linear wavelength. The corrections for the heat losses to the walls and into the growing spikes have been modeled separately. The rate of mass entrainment is obtained from the measurements of the rate of change of the thickness of the liquid slug as it is accelerated upwards. There is also some

noncondensible gas in the very short intermediate section, whose effects may be significant in the very early stages of the liquid slug displacements. The actual pressure histories are given in Seo (1987). It is assumed that the steam space containing falling and condensing droplets is sufficiently well mixed so that the steam is always at the local saturation temperature. This is the first attempt, as noted above, to actually model this process of condensation, although previous authors have also measured overall condensation rates. The agreement between theory and experiment is actually quite good, considering the uncertainties in this model and the precision of the experiment in these very fast mass transfer situations.

CONCLUSIONS

1. As expected, the start-time velocity, defined as the relative velocity of the lower and upper interfaces of an upwardly-accelerated water column, in the presence of steam condensation, is approximately proportional to the fourth root of the acceleration. The lower interface remains flat, although at long times, one might expect a Taylor-bubble shape in a round tube.
2. The estimated values of the droplet heat transfer coefficients show surprisingly good agreement between the experimental difficulties.
3. The work potential is reduced by a factor $\geqslant 2$ or more by steam condensation as compared to a noncondensable driver gas.

Acknowledgements—This work was supported by Grant CBT-8520364 from the National Science Foundation. Partial support from the Republic of Korea Army is also acknowledged with thanks.

REFERENCES

BANKOFF, S. G. 1959 On Taylor instability of plane surfaces. *Phys. Fluids* **2,** 576.

BANKOFF, S. G. & MASON, J. P. 1962 Heat transfer from the surface of a steam bubble in turbulent subcooled liquid stream. *AIChE Jl* **8,** 30–33.

BELLMAN, R. & PENNINGTON, R. H. 1954 Effects of surface tension and viscosity on Taylor instability *Q. Jl appl. Math.* **12,** 153–162.

BIRKHOFF, G. 1954 Taylor instability. Report No. LA-1862, Los Alamos Scientific Lab., Los Alamos, N.M.

CHANG, I. M. & BANKOFF, S. G. 1983 Nonlinear Taylor instability of a plane interface between two incompressible fluids with interfacial mass transfer. *AIChE Jl* **29,** 95–100.

CHANG, I. M. & BANKOFF, S. G. 1984 Nonlinear Taylor instability on a cylindrical vessel. *ASME Jl Fluid Engng* **106,** 380–384.

CHANG-MATEU, I. M. 1985 Entrainment and condensation effects in the acceleration of a liquid slug by an expanding gas or steam region. Ph.D. Thesis, Northwestern Univ., Evanston, Ill.

CHRISTOPHER, D. M. 1977 Transient development of a two-phase jet. Master's Thesis, Purdue Univ. West, Lafayette, Ind.

CORRADINI, M. L. 1978 Heat transfer and fluid flow aspects of fuel–coolant interactions. Ph.D. Thesis, MIT, Cambridge, Mass.

DIENES, J. 1978 Method of generalized coordinates and an application to Rayleigh–Taylor instability. *Phys. Fluids* **21,** 736–744.

EMMONS, H. W., CHANG, C. T. & WATSON, B. C. 1960 Taylor instability of finite surface waves. *J. Fluid Mech.* **177,** 77–193.

HSIEH, D. Y. 1979 Interfacial stability with mass and heat transfer. *Phys. Fluids* **22,** 1435–1439.

JACOBS, J. W., BUNSTER, A., CATTON, I. M. & PLESSET, M. S. 1985 Experimental Rayleigh–Taylor instability in a circular tube. *ASME Jl Fluids Engng* **107,** 460–466.

LEWIS, D. J. 1950 The instability of liquid surfaces when accelerated in a direction perpendicular to their planes II. *Proc. R. Soc.* **A202,** 81–96.

RATAFIA, M. 1973 Experimental investigation of Rayleigh–Taylor instability. *Phys. Fluids* **16,** 1207–1210.

RAYLEIGH J. W. 1900 *Scientific Papers*, Vol. II, p. 200 Cambridge, Univ. Press, U.K.

READ, K. I. & YOUNG, D. L. 1983 Experimental investigation of turbulent mixing by Rayleigh–Taylor instability. AWRE Report No. 011/83, Atomic Weapons Research Est., Aldermaston, U.K.

SEO, J. S. 1987 Entrainment and condensation effects in the upward acceleration of a liquid column. Ph.D. Thesis, Northwestern Univ., Evanston, Ill.

TAGHAVI-TAFRESHI, K. & DHIR, V. K. 1980 Taylor instability in boiling, melting, and condensation or evaporation. *Int. J. Heat Mass Transfer* **23,** 1433–1445.

TAYLOR, G. 1950 The instability of liquid surfaces when accelerated in a direction perpendicular to their planes I. *Proc. R. Soc.* **A201,** 192–196.

TOBIN, R. J. & CAGLIOSTRO, D. J. 1978 Effects of vessel internal structures on simulated HCDA bubble expansions. SRI Project PYU-3929, Technical Report No. 5., Stanford Research Inst., Palo Alto, Calif.